UNCLASSIFIED

③

CRDV RAPPORT 4075/77
DOSSIER: 3634C-004
AOÛT 1977

DREV REPORT 4075/77
FILE: 3634C-004
AUGUST 1977

LABORATORY SIMULATION OF ATMOSPHERIC TURBULENCE

FOR OPTICAL PROPAGATION STUDIES

L.R. Bissonnette

Centre de Recherches pour la Défense

Defence Research Establishment

Valcartier, Québec

BUREAU - RECHERCHE ET DEVELOPPEMENT
MINISTÈRE DE LA DÉFENSE NATIONALE
CANADA

RESEARCH AND DEVELOPMENT BRANCH
DEPARTMENT OF NATIONAL DEFENCE
CANADA

NON CLASSIFIÉ

(6)

LABORATORY SIMULATION OF ATMOSPHERIC TURBULENCE

FOR OPTICAL PROPAGATION STUDIES

by

(10) L.R. Bissonnette

(11) Aug 77   (12) 47 p.

CENTRE DE RECHERCHES POUR LA DEFENSE

DEFENCE RESEARCH ESTABLISHMENT

VALCARTIER

Tel: (418) 844-4271

Québec, Canada   August/août 1977

404 945

RESUME

On démontre qu'une cuve remplie d'eau de 1.5 m de longueur sur
40 cm de largeur et 60 cm de profondeur, réchauffée par le bas et refroidie
par le haut, constitue une technique simple pour simuler avec précision
et à l'échelle du laboratoire l'effet des turbulences atmosphériques sur
la propagation des ondes lumineuses. L'indice de réfraction possède une
structure de turbulence similaire à celle de l'atmosphère; plus particu-
lièrement, le modèle de Kolmogorov relatif au sous-domaine inertiel est
très bien vérifié. On retrouve dans le milieu de simulation les mêmes
particularités que dans l'atmosphère en ce qui a trait à la densité
spectrale de l'intensité lumineuse et aux phénomènes de saturation et
supersaturation de la variance de l'intensité. La loi d'échelle est la
même dans les deux cas et les distances caractéristiques de propagation
sont typiquement réduites par un facteur 300 à 400. (NC)

ABSTRACT

Accurate simulation, on a laboratory scale, of atmospherically
induced scintillation phenomena is achieved by creating an unstable
vertical temperature gradient in a 1.5-m long, 40-cm wide and 60-   p
tank filled with water. The turbulent index of refraction has a
statistical structure similar to that of the atmosphere; in particular,
the Kolmogoro's inertial subrange model is verified. The turbulent
irradiance data in the simulation medium have the same features respecting
power spectrum, saturation and supersaturation and obey the same theoretical
scaling law as in the atmosphere. Typically, the characteristic propaga-
tion distances are reduced by a factor of 300 to 400. (U)
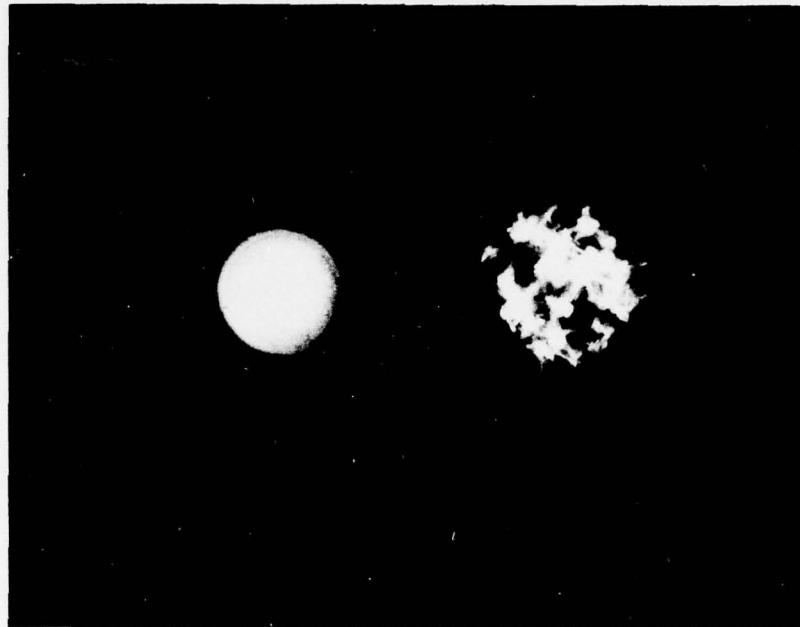
UNCLASSIFIED
ii

TABLE OF CONTENTS

FIGURE 1 - Comparison of instantaneous irradiance patterns of a 25-mm
diameter collimated He-Ne laser beam propagating under
homogeneous and turbulent conditions. Exposure time was
1/50s. Left: diffraction limited pattern. Right: turbulence-
distorted pattern, $2\sigma_\chi = 4$.

1.0 <u>INTRODUCTION</u>

Military applications of optical and infrared laser beams of any power or energy level are perturbed by atmospheric turbulence. The seriousness of this problem depends, of course, on the particular application but the turbulence-induced distortion may become very extensive, as illustrated in Fig. 1 where the instantaneous irradiance pattern of a laser beam propagating in turbulence is compared with its diffraction limited pattern at the same position. The turbulence-distorted beam irradiance is broken up in several patches and the positions of these patches vary continuously in a random fashion. Therefore, it is important to understand and model the mechanisms leading to such complete distortion to assess the performance of military laser systems and to optimize adaptive or compensating optical devices.

Well-known analytical treatments of scintillation phenomena were derived from first order perturbation theories, for example the Born and Rytov methods outlined in Refs. 1 and 2. The results derived from these models are generally well verified but they apply only under weak scintillation conditions. Models valid in the strong scintillation limit have recently been proposed, e.g. Refs. 3-5. These models are reasonably successful but they all rely on some form of empiricism that has to be carefully corroborated by experiments. A model applicable for arbitrary propagation range and turbulence strength was also developed at DREV (Ref. 6). Its format is substantially different in that it deals directly with the differential equations for the statistical moments of the wave amplitude rather than with approximated integral relations involving these moments as is generally the case in other models. The principal advantage of this approach is that the turbulence effects can be easily incorporated in our computer code (Refs. 7-8) for the prediction of thermal blooming of high-power laser beams with an estimated factor-of-two increase in computation time only. However, specialized data not available elsewhere are required to verify the constitutive hypotheses and to specify the empirical constants, hence the need for an independent experimental program.

Experimentation in the atmosphere is subject to many constraints. A convenient site has to be found which, for the purpose of meaningful comparison with theory, must be homogeneous over a distance of several hundred meters. But, most importantly, the experimenter has no control over the prevailing meteorological conditions not to mention that the latter can change considerably during the required experimentation time. Consequently, systematic probing of two-point statistical functions, such as the index structure function and the irradiance correlation function, is practically impossible unless a large number of measuring channels can be set up or simplifying approximations made. To avoid such difficulties, we designed a laboratory experiment to simulate atmospheric turbulence. The requirements are that the known characteristic properties of the structure of atmospheric turbulence be preserved and that the resulting scintillation phenomena be scaled down to laboratory dimensions. The purpose of this document is to demonstrate that our simulation apparatus satisfies very well these requirements.

The simulation apparatus is described in detail in Section 2.0. Section 3.0 shows that the structure function and frequency spectrum of the turbulent refractive index measured in the simulation medium have the inertial subrange which is characteristic of the structure of turbulence in the lower atmosphere and which is predicted by the theory of equilibrium turbulence. One-point irradiance statistics are discussed in Section 4.0 where simulation results are shown to agree with atmospheric data and theoretical predictions.

This work was performed at DREV between January and September 1976 under PCN 34C04 (formerly 07E04) "Propagation of Laser Beams".

2.0 SIMULATION APPARATUS

The turbulent medium of propagation is artificially produced by creating an unstable vertical temperature gradient in a tank filled with water. Water is used mainly because of the rapid variation of its refractive index N with respect to temperature T. Typically, dN/dT is equal to $10^{-4}/°C$ in water compared with $10^{-6}/°C$ in air at standard temperature and pressure. Thus, one can consider only small temperature fluctuations, of the order of $1°C$ or less, and still create refractive index fluctuations 100 times stronger than those in the real atmosphere. Therefore, it is possible to reduce to laboratory dimensions the propagation distances characteristic of the turbulence forward-scattering phenomena without unduly disturbing the average properties of the medium by imposing large temperature variations. This is important to achieve a good simulation of the atmosphere where the random fluctuations of its thermodynamic properties are indeed small enough to be considered linear. The approach chosen here is also very attractive since the physics governing the production of the index irregularities is basically the same as in the real atmosphere, namely the presence of a warmer boundary at the bottom layer of a fluid in the gravitational field; moreover, no artificial stirring, mixing or blowing, etc... is used. Finally, water is very practical to work with; it is easily available and, owing to its large thermal inertia, it is less likely to be affected by the ubiquitous environmental temperature fluctuations in the laboratory room.

Water is contained in a Plexiglass tank measuring 1.5-m long, 40-cm wide and 60-cm deep. Heating is provided by twenty-four 1200-Watt electrical heaters positioned transversely at an equal distance from each other and at 7 cm above the floor of the tank. The tubular electrical elements have a 15-mm external diameter. They are electrically connected to give equal current in each resistor and the overall power input is continuously variable between 0 and 7.5 kW. The heat supplied to the lower boundary of the medium is balanced by circulating cold tap water

in a heat exchanger located 2 cm below the free surface. Water is not replaced except for losses by evaporation. This has the advantage of keeping its gas content, after one or two days of operation, to almost zero. Thus, the medium remains virtually free from air bubbles that would perturb the turbulence scintillation phenomena. A filtering and demineralyzing system is turned on between measurement periods; this is sufficient to keep the water and tank clean over intervals of many weeks.

The arrangement described in the preceding paragraph led to the formation of large convection cells. Roughly, these had the dimension of the height between the heaters and the heat exchanger and therefore they destroyed the homogeneity of the propagation medium. To prevent this circulation, plastic dividers, 6 cm apart, were installed transversely in the lower half of the tank and longitudinally in the upper half. The two sets of dividers are   ated in the middle of the tank by a 15-cm deep free region which   as the propagation test volume. The center of the test re   is 25 cm above the electrical heaters and approximately 22 cm below the water surface. The propagation distance is increased by folding mirrors positioned immediately outside of the tank to minimize the optical path in air. Transmission at both ends of the tank is made through three equally spaced 7-cm diameter optical windows which allow a practical propagation distance in water equal to 7.5 m. The total beam power is depleted by water absorption, Rayleigh scattering, reflection from window surfaces and losses by the deflection mirrors, all linear effects independent of, and not affecting, the turbulent irradiance structure.

The simulation tank is shown in Fig. 2.

In the following sections, the temperature or refractive index data are referred to the right-hand coordinate system (X, Y, Z) where X is the height measured from the position of the electrical heaters and Y and Z are the transversal and longitudinal coordinate in

the horizontal plane inside of the tank. The irradiance measurements are referred to the right-hand coordinate system (x, y, z) where x and y are the coordinates in the plane normal to and centered on the optical axis of the laser (y being in the vertical direction) and z is the propagation distance along the laser beam measured from the point where the beam first enters the water.
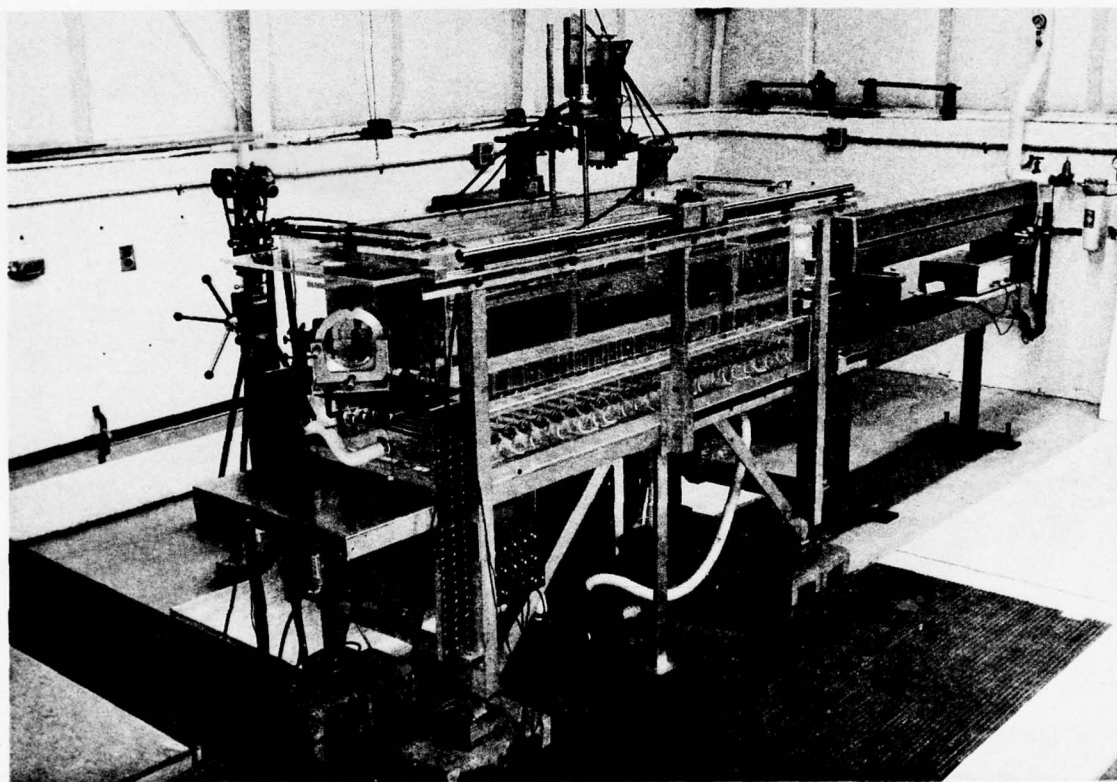

FIGURE 2 - Photograph of simulation apparatus.

3.0 REFRACTIVE INDEX STATISTICS

The aspect of turbulence which is of interest to optical propaga-
tion is the random variation of the refractive index of the medium. Since
the fluctuations of the thermodynamic properties of the simulation medium
are kept small, the refractive index variations can be linearly related to
the temperature variations as follows:

$$n = \frac{dN}{dT} \, \theta \, , \tag{1}$$

where T and N are the average temperature and refractive index and θ and n,
the centered random temperature and refractive index fluctuations respec-
tively. Ref. 9 gives for water:

$$10^5 (N-1.332156) = -8.889 \, (T-20) - 0.1610 \, (T-20)^2 \, . \tag{2}$$

where T is expressed in °C.

3.1 Temperature Measurements

The random temperature fluctuations are measured by temperature
dependent fine resistors of low thermal inertia inserted in a Wheatstone
bridge. Both the sensors and the electronic bridge are commercially
made. The sensor is a fiber-film probe which consists of a nickel
film deposited on a 70-μm diameter quartz fiber. The sensitive length
of the film is 1.25 mm. Electrical insulation and water protection are
provided by a quartz overcoating approximately 2 μm thick. Typically,
the sensor resistance at 20°C, R_{20}, is 10 ohms and its temperature
coefficient, $\alpha_{20} = (\Delta R/R_{20})/\Delta T$, is 0.35%/°C. The Wheatstone bridge is
operated in the constant current mode and is specifically designed to
measure rapid temperature fluctuations. The DC level of the signal
is removed by a high pass filter with a 3 dB frequency cutoff of 0.015 Hz

and the remaining random part is passed through a variable amplifier. The precision on temperature measurements is about 1% of the peak variations or better than 10% of the typical standard deviation of the turbulent fluctuations. Two such systems are used for simultaneous temperature measurement at two different locations in the turbulent medium.

The voltage-temperature sensitivity of the system is proportional to the sensor current. However, since the sensor temperature increases with the sensor current, the latter should not exceed a certain limit as this would cause the sensor to become sensitive to flow velocities as well, which would distort the temperature measurements. To determine this limit, the sensor resistance was measured as a function of the sensor current at various sensor velocities in non-turbulent water. For sensor currents inferior or equal to 3 mA, no detectable resistance changes were observed at velocities smaller than 10 cm/s. The characteristic fluid velocity in the turbulent water is given by the upwelling velocity of the heated eddies, i.e. $V_g = \sqrt{\beta g d\theta}$ where β is the coefficient of thermal expansion of water, g the gravitational acceleration, d the representative diameter of the eddies and θ their excess temperature. As will be seen later, the eddy diameter and the excess temperature are of the order of 1 cm and 1°C respectively, which gives $V_g \simeq 0.5$ cm/s. This value is well corroborated by semi-quantitative observations of the rising velocities of dyed water. All temperature data reported in this document were obtained with a sensor current near 3 mA and, therefore, the results are certainly not affected by kinetic turbulence.

The upper frequency limit of the electronic system operated with fiber-film probes of the type used in this experiment is quoted by the manufacturer to be a few hundred hertz. Since this amply covers the frequency bandwidth of a few hertz of the temperature fluctuations to be investigated in the present research program, no attempt was made to determine the actual frequency cutoff of our system.

3.2 Instantaneous Temperature, Lapse Rate and Temperature Variance

A typical recording of the temperature difference between two points separated by 2.5 mm is shown in Fig. 3. The heating power was 6.0 kW and the sensors were located 25 cm above the electrical heaters. The peak temperature variations were of the order of ±1°C.

Figure 3 illustrates quite clearly one important characteristic of the structure of thermal turbulences: intermittency. As indicated, periods of fairly quiet temperature fluctuations are immediately followed by periods of strong turbulent activity and vice versa. This phenomenon is routinely observed in the atmosphere and is discussed, for example, in Refs. 10-13. In particular, there is a definite similarity between the recording of Fig. 3 and those of Fig. 2 of Ref. 12 and of Fig. 1 of Ref. 13 except, of course, for the differences in the time scales which obviously are to be expected. The intermittency of the turbulent signal is partly explained by the plume structure of the convectively unstable lower atmosphere whereby the heated and thermally nonuniform air parcels rise from the ground in vertically elongated columns of relatively sharp boundaries amid more uniform cool sinking air. Fig. 3 shows that an equivalent structure exists in the simulation medium. Indeed, depending on whether the fixed temperature sensors are located inside or outside these vertical columns which move about in a slow unsteady fashion, they measure strong or weak temperature fluctuations. Hence, Fig. 3 constitutes preliminary qualitative evidence that the structure of the simulated turbulence is similar to that of the lower atmosphere.

Two different types of average temperature variations are observed. First, there are very-long-term homogeneous variations caused by the ambient laboratory conditions. These variations could have been offset by continuously adjusting the flow rate in the heat exchanger by feedback circuitry. However, sample measurements of the structure function made under different conditions indicated that this homogeneous average
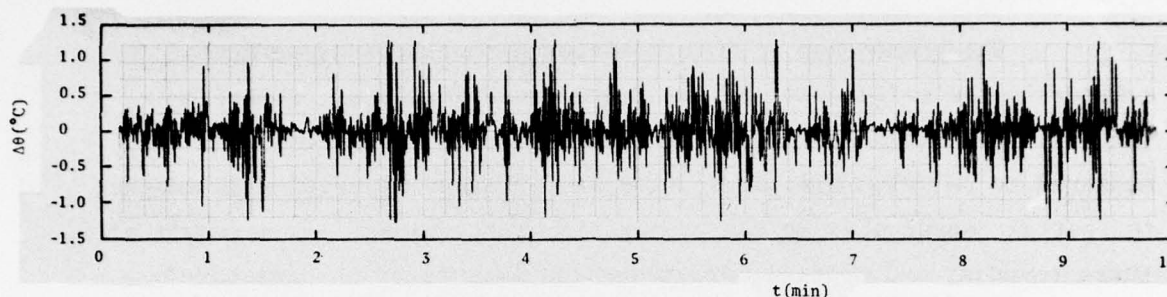
FIGURE 3 - Typical time-recording of instantaneous temperature
difference between 2 points separated by 2.5 mm. Heating
power was 6.0 kW and sensors were located 25 cm above heaters.

temperature drift, of the order of $\pm0.5°C/h$ or less, had no measurable
effects on the structure of the thermal turbulences. The average
temperature was never allowed to wander by more than $\pm0.2°C$, which was
accomplished by manual adjustments of the cooling flow rate. A one-hour
settling time was always allowed before initiating measurements. Second,
there are long-term inhomogeneous random variations of the average tem-
perature which are most likely connected with the intermittency
phenomenon described in the preceding paragraph. These fluctuations, of the
order of the temperature standard deviation, occur on a scale of a few
minutes in the temporal domain and of a few centimeters in the spatial
domain. They are characteristic of the turbulence and therefore
unavoidable.

The decrease of the average temperature with height, called
the lapse rate, constitutes a measure of the hydrostatic stability
of a fluid layer in the gravitational field. Attempts were made to
measure the lapse rate in the simulation tank but they were all
inconclusive. The unsteady and inhomogeneous long-term temperature
variations turned out to be larger than the average temperature
difference over the 15-cm height available for measurements; thus, no
reproducible gradient could be obtained. Hence, it is concluded that
the lapse rate is smaller than approximately $0.01°C/cm$ in all three
experimental situations defined in Table I. For comparison purposes,
the adiabatic lapse rate $g/C_p = 2.3\times10^{-5}°C/cm$.

The phenomenon of intermittency also causes experimental
scatter in the measurement of the temperature variance. Relative
temporal fluctuations of the temperature standard deviation were
measured to be 20%. Similar scatter was likewise observed with respect
to spatial coordinates in the propagation test volume. As a result of
these temporal and spatial variations and because of the relatively
small height (15 cm) of the test volume, no reproducible vertical
gradient of the temperature variance could be measured.

It would seem from the results reported in the foregoing
paragraphs that the medium is neither homogeneous nor stationary.
However, the temporal and spatial scales of the observed variations
suggest that they are linked to the phenomenon of intermittency. Since,
as discussed in Ref. 13, these long-term fluctuations resulting from
intermittency are not basically related to questions of homogeneity
and stationarity, we conclude that the simulation medium can in fact
be described as statistically homogeneous and stationary.

Relevant average properties of the medium are given in
Table I. All standard deviation values quoted are the results of
averaging over many experiments.

TABLE I

Dimensional Parameters Describing Experimental Conditions

Heating Power kW	Average Temperature (T) °C	Temperature Standard Deviation (σ_θ) °C	Index Standard Deviation (σ_n)	Turbulence Strength (C_n) $m^{-1/3}$
4.6	24	0.100	1.11×10^{-5}	0.73×10^{-4}
6.0	27	0.135	1.50×10^{-5}	0.96×10^{-4}
7.5	30	0.155	1.72×10^{-5}	1.24×10^{-4}

3.3 Index Probability Distribution

The thermal fluctuations associated with the turbulence effects
relevant to optical propagation in the atmosphere are characterized by
probability distributions which differ markedly from normality (Refs. 12-13).
Figure 4 shows that the same observation applies to our simulation medium.
In this figure, the measured probability distribution of the temperature
difference $\Delta\theta$ between two sensors separated by 1.5 mm is compared with a
normal curve. The distribution is computed from a single, 22-min long
record sampled at a rate of 2.5 Hz, which is approximately equal to one
half of the signal bandwidth. The data points follow closely enough the
normal curve for small $\Delta\theta$ values but largely deviate in the tails. These
results are in good agreement with the atmospheric data of Refs. 12-13 and,
therefore, constitute further evidence that the structure of the
turbulent refractive index of the atmosphere is well simulated in our
laboratory experiment. Exact corroboration regarding the index probability
distribution is, however, not possible at this time since, on the one hand,
experiments in the atmosphere have yielded distributions which are mostly
amorphous and, on the other hand, theoretical models are practically
unconcerned with this problem. Systematic probability investigations
will be pursued in later experiments.

3.4 Index Structure Function and Frequency Spectrum

3.4.1 Background

A very important result on the statistical structure of
homogeneous mechanical turbulence is the Kolmogorov-Obukhov theory
discussed at length in Ref. 14. This theory postulates that, if the
characteristic turbulent Reynolds number is sufficiently large, there
exists a range of wave numbers for which the Fourier coefficients
are statistically steady, isotropic and independent of the structure of
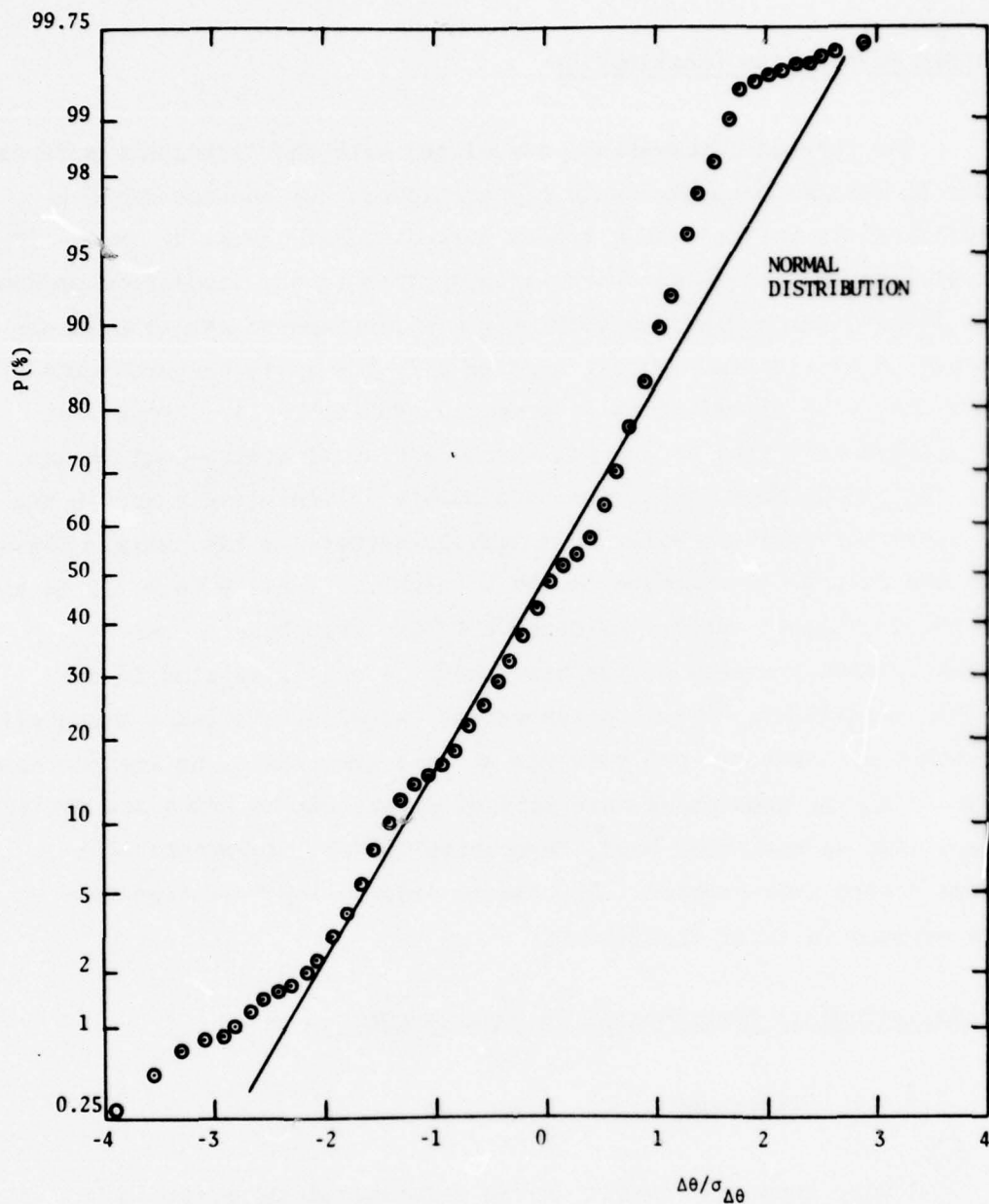the energy-containing eddies, i.e. the Fourier coefficients at the small

FIGURE 4 – Probability distribution of normalized instantaneous temper-
ature difference $\Delta\theta/\sigma_{\Delta\theta}$ between two points 1.5 mm apart.
Heating power was 6.0 kW. Solid line represents a normal
distribution. $\sigma_{\Delta\theta}$ was determined directly from the tempera-
ture record and not from a best fit to the normal curve.

wave number end of the spectrum. This range is called the equilibrium range; it is self-adjusting through the action of the inertia forces and depends only on the energy input rate at small wave numbers and on the energy dissipation rate by viscosity at high wave numbers. Moreover, if the Reynolds number is large enough so that the energy-containing eddies and the dissipation eddies are widely separated on the wave number scale, there may exist a subrange in which negligible dissipation occurs. If this is the case, the transfer of energy by inertia forces from large to small eddies, or from small to large wave numbers, remains the only or the dominant dynamical process in this subrange; hence, the appellation inertial subrange. From dimensional analysis, this condition implies that, within the inertial subrange, the spectra of all three velocity components are proportional to the 5/3 power of wave number or frequency and that the structure function varies as the 2/3 power of the lag distance. It can be shown (Ref. 1) that the statistical structure of turbulent conservative passive additives, such as temperature or refractive index which are of interest here, also obeys the law of the inertial subrange under the same conditions.

Estimates of the scales of the relevant dynamical processes reveal that the equilibrium conditions justifying the existence of an inertial subrange are normally satisfied in the lower atmosphere. Experimental results on the turbulent temperature or refractive index summarized by Tatarskii (Refs. 1-2) are in excellent agreement with the power laws of the inertial subrange. There are some few instances where measurements differ from this model. For example, in Ref. 12, the temperature structure function measured 1.5 m above ground displays a slope of only 1/2 for separation distances smaller than 30 cm which should normally fall within the inertial subrange. Also, in Ref. 15, it is argued that optical phase-front distortion data taken 2.5 m above ground would be better modelled by assuming an index structure function following a power law with an exponent as low as 1/3. However, such results are not generalized and are probably explained

by special experimental conditions. In any case, it is widely accepted by
most workers that the inertial subrange and the corresponding power laws are
well verified and constitute the most practical characterization of the
turbulent refractive index in the lower atmosphere. It is therefore
essential that the inertial subrange model be verified in our laboratory
experiment. This will insure that the structure of the simulated turbulence
is the same as in the lower atmosphere or, more specifically, that the wave
number domain where most of the turbulent energy is contained is independent
of the wave-number domain where most of the dissipation occurs. The
experimental data of the following sections show that the turbulence in
the simulation medium has indeed an inertial subrange.

3.4.2 Measurement Techniques

The statistical property of a turbulent medium which is most
relevant to optical propagation is the index structure function. This
function is defined as follows:

$$D_n(r_1, r_2) = \langle (n(r_1) - n(r_2))^2 \rangle, \qquad (3)$$

where $n(r_i)$ is the instantaneous index of refraction at location r_i (i=1,2)
and where the angular brackets designate ensemble averaging. Since the length
scale of the structure function is generally small compared with the
characteristic environmental length scale, it is justified to assume
statistical homogeneity and statistical isotropy. Under these approxima-
tions, the structure function D_n depends on the magnitude of the vector
difference only, i.e.:

$$D_n(r_1, r_2) = D_n(|r_2 - r_1|). \qquad (4)$$

Therefore, it is not necessary to take data in several directions of
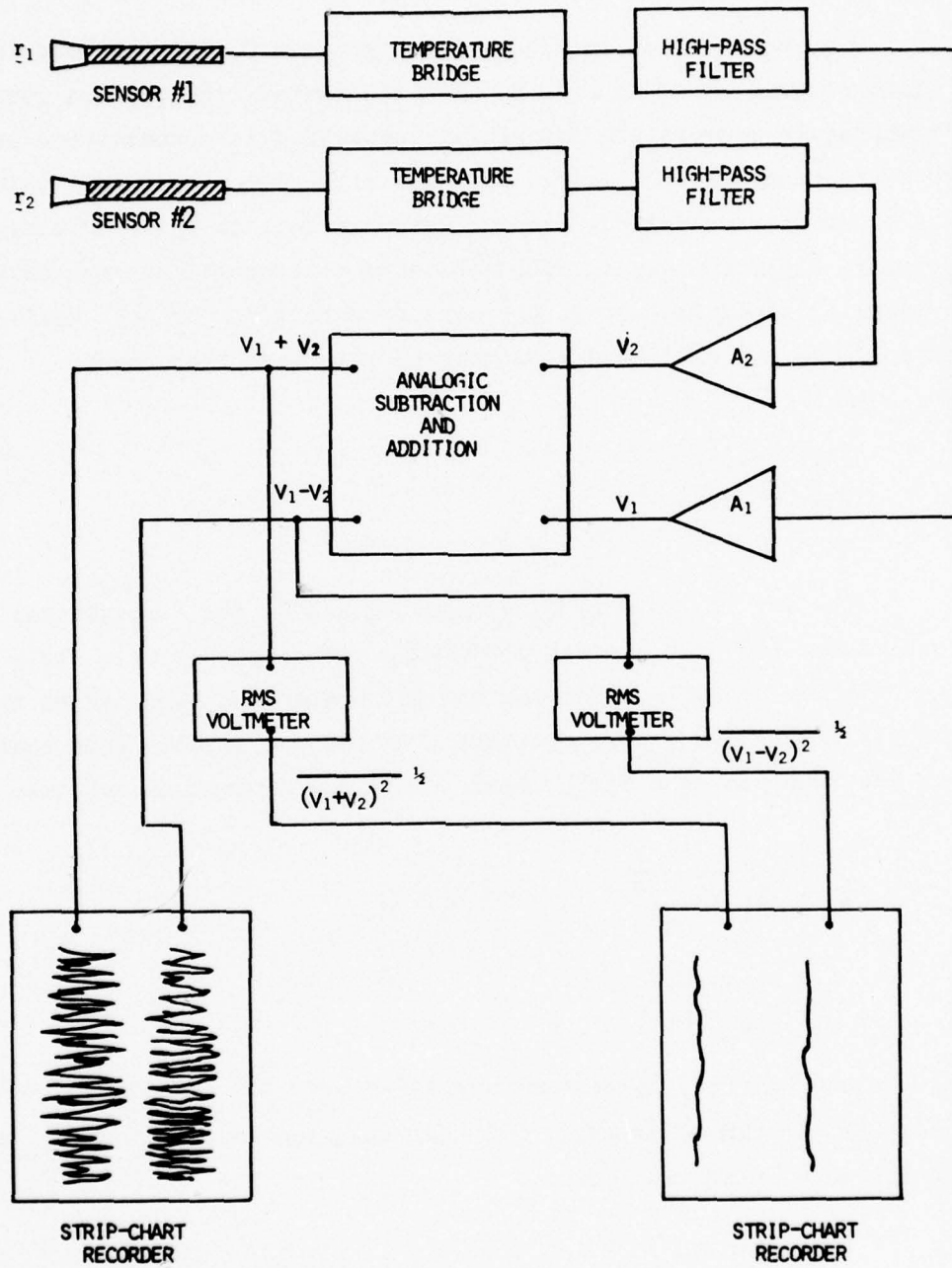separation, a single series of measurement points along a line is sufficient.

FIGURE 5 - Block diagram showing method of measurement of refractive
index structure function.

The method used to measure the function D_n is best described by
the block diagram shown in Fig. 5. As illustrated, the signals from the
two temperature sensors are identically processed in a Wheatstone bridge,
filtered to remove the DC level, and amplified. Two electrical voltages
V_1 and V_2 are thus obtained which are proportional to the fluctuating
temperature $\theta(r_1)$ and $\theta(r_2)$. The constants of proportionality can be
made equal by simply adjusting the sensor current and/or the ampli-
fication factor of one channel with respect to the other; hence:

$$V_1 = C \, \theta(r_1) \, , \tag{5}$$

$$V_2 = C \, \theta(r_2) \, . \tag{6}$$

The two instantaneous voltages V_1 and V_2 are electronically added
and subtracted and both sum and difference are displayed on a strip chart
for qualitative analysis. The sum and difference are also fed to two RMS
voltmeters with a 100-s time constant. The output signals from these
meters are recorded on a strip chart. They are denoted as follows:

$$e_s = \overline{(V_1 + V_2)^2}^{\frac{1}{2}} \, , \tag{7}$$

$$e_d = \overline{(V_1 - V_2)^2}^{\frac{1}{2}} \, , \tag{8}$$

where the overbar designates time averaging over the 100-s integration
constant of the RMS voltmeter. One-hour long records of e_s and e_d are
taken for each separation point.

To obtain results which more closely approximate ensemble averages
as encountered in equation (3), the RMS data are averaged over the length
of the one-hour long records. Hence, the temperature correlation function is
given by:

$$B_\theta \equiv \frac{<\theta(\underline{r}_1)\,\theta(\underline{r}_2)>}{\frac{1}{2}\{<\theta(\underline{r}_1)^2>+<\theta(\underline{r}_2)^2>\}} \simeq \overline{\overline{\left(\frac{e_s^2 - e_d^2}{e_s^2 + e_d^2}\right)}} \quad , \tag{9}$$

and the temperature structure function by:

$$D_\theta \equiv <(\theta(\underline{r}_1) - \theta(\underline{r}_2))^2> \simeq \frac{1}{2C^2}\,(1-B_\theta)\,\overline{\overline{<(e_s^2 + e_d^2)>}} \quad , \tag{10}$$

where the double overbars denote time averaging over the one-hour long RMS records and where the angular brackets in equation (10) represent averaging over all available such records. From equation (1), the refractive index correlation and structure functions are related to B_θ and D_θ as follows:

$$B_n = B_\theta \, , \tag{11}$$

$$D_n = \left(\frac{dN}{dT}\right)^2 D_\theta \, . \tag{12}$$

The measured statistical standard deviation errors for B_n and D_n are smaller than 5%. These relatively small errors compared with the 20% experimental scatter on the temperature variance are due to the constant normalization of the RMS signals shown in equation (9) which compensates for fluctuations resulting from intermittency.

Computations of frequency spectra are performed digitally. The analog signal is digitized and momentarily stored in a 5120-word buffer memory. Transfer of the data to the central computer is done in time sharing mode using a standard CRT display computer terminal. All subsequent data handlings are done by software. Calculations of auto-correlation functions and frequency spectra of these finite length discrete records are carried out according to the method described by Blackman and Tukey (Ref.16).

3.4.3 Results

Measurements of the refractive index structure function were performed for three different values of heating power: 4.6, 6.0 and 7.5 kW. The results are plotted on log-log graphs in Figs. 6-8. The displacement $\rho = \sqrt{Y^2 + Z^2}$ between the sensors is in the horizontal plane. The 2/3 power law of the inertial subrange fits the data very well for a range of separation values comprised between approximately 2 and 6 mm. Deviations at smaller distances are toward a greater slope in agreement with theory which predicts a quadratic law at zero separation (Refs. 1-2). However, exact verification of the quadratic law is not possible since the length of the temperature sensors exceeds their separation distance in this region leading to ambiguity in the interpretation of the temperature data. The structure function levels off for separations greater than 6 mm and correlation vanishes near 20 mm. Homogeneity of the simulation medium with respect to the structure function is excellent. Differences between sample measurements made at various locations in the propagation test volume are well within experimental errors.

The results of Fig. 7 were obtained in earlier experiments when only one RMS voltmeter was available. Hence, only the voltage difference $(V_1 - V_2)$ could be processed which means that the constant normalization of the data shown in equation (9) was not possible. This explains the somewhat greater experimental scatter observed in Fig. 7 but it also demonstrates the excellent degree of reproducibility of specific experimental conditions. Indeed, every single data point in Figs. 6-8 represents a full hour of recording time so that Fig. 7 alone has required several days of experimentation during which operating conditions had to be reproduced from day to day.

The range of separation values over which the 2/3 power law of the inertial subrange is verified may appear somewhat small. However, it is consistent with the nature of the turbulent medium. Indeed, flow visualization suggests that the largest eddies, or the energy-containing

eddies, are of the order of 1 to 3 cm in diameter while calculations based on estimates of the turbulent kinetic energy dissipation rate give something of the order of 1 mm for the size of the energy-dissipating eddies. Since the inertial subrange is defined to exist between these two extremes provided they are sufficiently separated, the observed 2- to 6-mm range for the 2/3 power law is in excellent agreement with theoretical prediction. Although this domain is narrow, its mere existence is sufficient to demonstrate the independence between the energy-containing and the energy-dissipating eddies which is a necessary condition to achieve statistical similarity of the turbulent refractive index.

Since the structure of the turbulent refractive index in the lower atmosphere obeys the inertial subrange model, the 2/3 power law is widely used to characterize the turbulent medium in optical propagation problems. In the inertial subrange, the index structure function is given by:

$$<(n(\underline{r} + \varrho) - n(\underline{r}))^2> = C_n^2 \rho^{2/3} \tag{13}$$

The constant of proportionality C_n^2 is called the index structure parameter. C_n has the dimension of a length to the minus 1/3 power and serves almost universally to define turbulence strength in optical applications. According to Figs. 6-8, C_n is equal to 0.73×10^{-4} $m^{-1/3}$, 0.96×10^{-4} $m^{-1/3}$ and 1.24×10^{-4} $m^{-1/3}$, respectively. These values are summarized in Table I along with other dimensional parameters. By comparison, the atmospheric turbulence strength is classified as follows (Ref. 17): weak turbulence $C_n = 8 \times 10^{-9}$ $m^{-1/3}$, intermediate turbulence $C_n = 4 \times 10^{-8}$ $m^{-1/3}$, and strong turbulence $C_n = 5 \times 10^{-7}$ $m^{-1/3}$. Hence, our simulation apparatus can produce turbulence conditions approximately 200 times stronger than strong atmospheric turbulence. C_n is proportional to (dN/dT) $K^{1/2}/\epsilon^{1/6}$, where K is the rate at which the temperature-squared inhomogeneities are levelled out in the smallest eddies and ϵ is the rate of dissipation of the turbulent kinetic energy. Comparing our results

with the typical atmospheric values in the light of this scaling formula, we see that the two-order-of-magnitude increase in C_n observed in the simulation medium is mostly due to the two-order-of-magnitude difference in the proportionality constant dN/dT which is independent of turbulence. Therefore, the important turbulence rates K and ϵ are substantially of the same order of magnitude in both cases, which could explain, at least partially, why we are able to achieve good similarity with regard to the structure of turbulence.

Typical frequency spectra of the refractive index $S_n(f)$ normalized by the index variance are shown in Figs. 9-10. Each spectrum was computed from a single discrete record of the instantaneous index obtained on different occasions for the same heating power of 6.0 kW. In the case of Fig. 9, the record length was 10.5 min and the sampling rate, 8 Hz; for Fig. 10, these parameters were 8 min and 10 Hz respectively. In both instances, the spectrum satisfies very well the minus 5/3 power law of the inertial subrange over approximately one decade of the frequency domain, i.e. 0.2-2 Hz. Beyond this range, the spectrum decays faster with increasing frequency, also in accordance with theory. These results are in good agreement with the atmospheric data, for instance those of Refs. 2 and 18.

The combined experimental results of Figs. 6-10 show quite satisfactorily that the turbulent refractive index fluctuations in the simulation medium have an inertial subrange. This is a very important result since the inertial subrange model is well verified in the atmosphere and is almost universally used to characterize atmospheric turbulence in optical propagation problems.
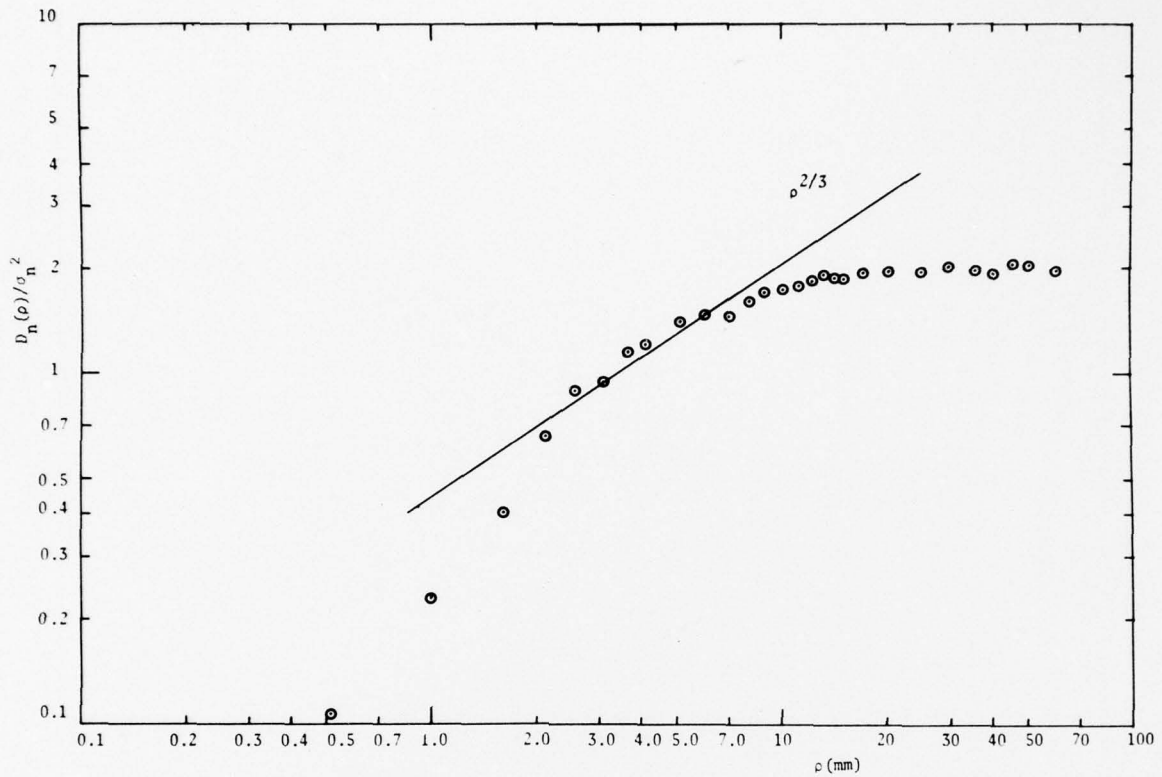
FIGURE 6 - Normalized refractive index structure function D_n/σ_n^2 versus separation distance ρ for a heating power of 4.6 kW. Solid line is Kolmogorov's 2/3 power law model for inertial subrange.
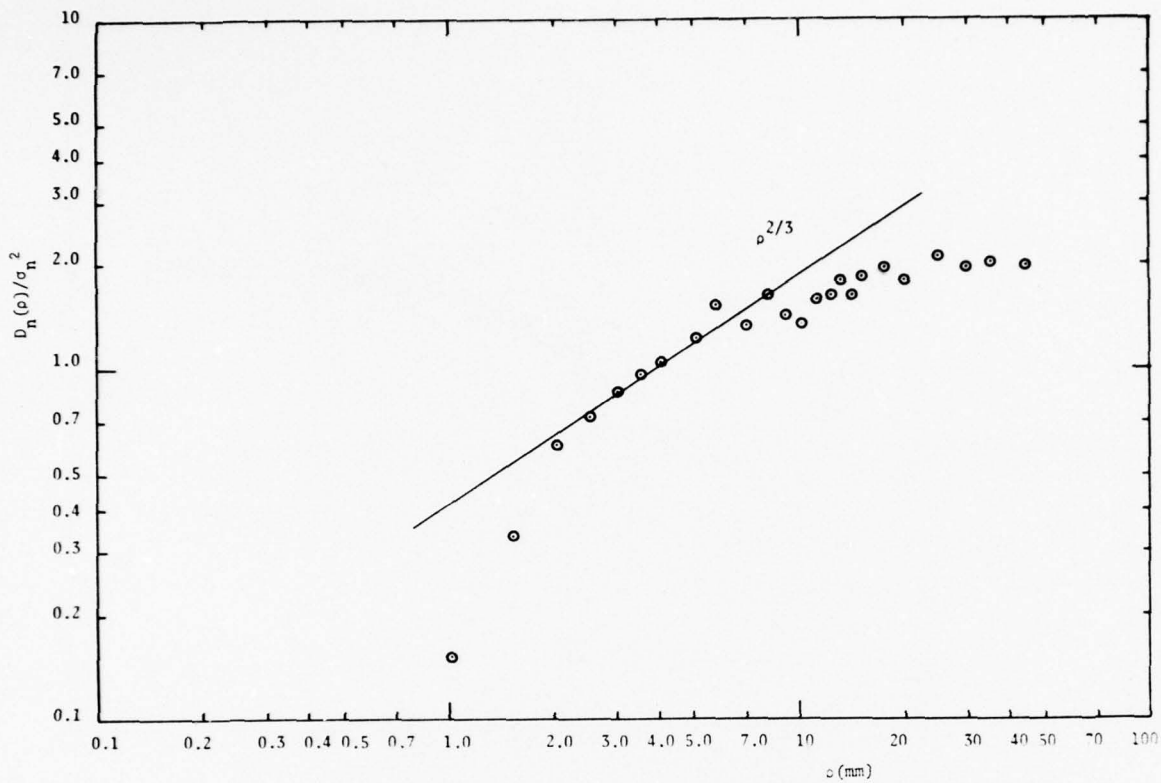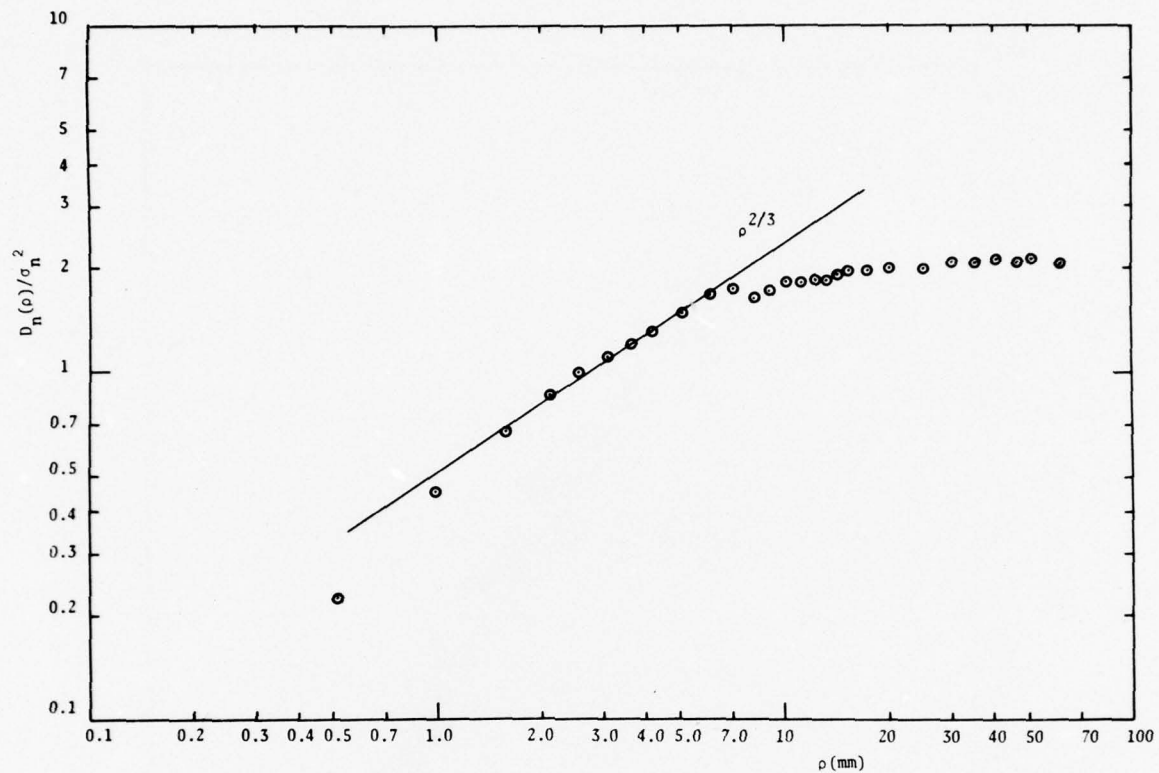
FIGURE 7 - Normalized refractive index structure function D_n/σ_n^2 versus
separation distance ρ for a heating power of 6.0 kW. Solid
line is Kolmogorov's 2/3 power law model for inertial subrange.

FIGURE 8 - Normalized refractive index structure function D_n/σ_n^2 versus separation distance ρ for a heating power of 7.5 kW. Solid line is Kolmogorov's 2/3 power law model for inertial subrange.

$S_n(f)/\sigma_n^2 \ (Hz^{-1})$

$f^{-5/3}$

f(Hz)
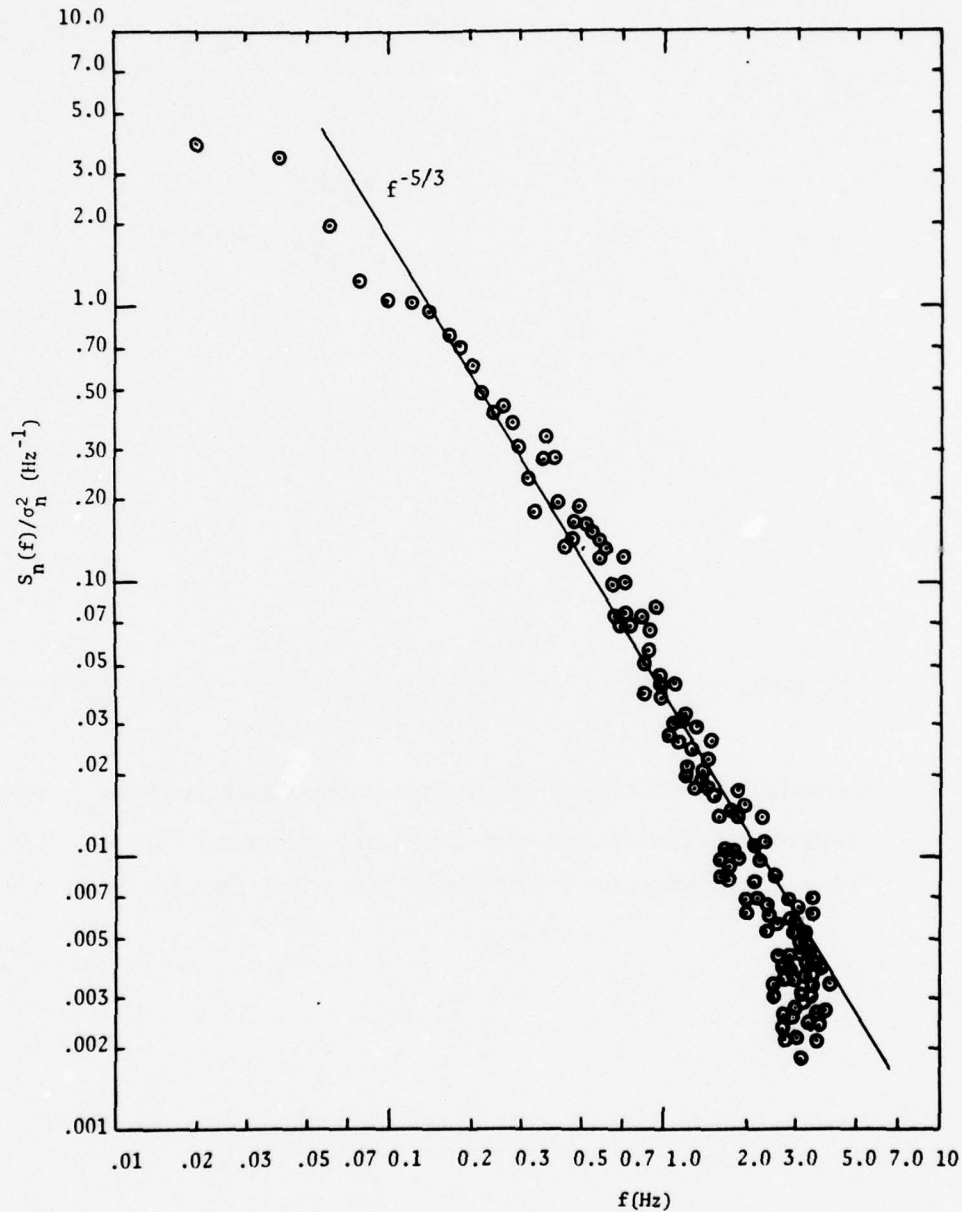
FIGURE 9 - Typical refractive index power spectrum $S_n(f)/\sigma_n^2$ computed
from a single 10.5-min long record sampled at a rate of 8 Hz.
Folding or Nyquist frequency is 4 Hz and elementary frequency
band 0.02 Hz. Heating power was 6.0 kW. Solid line is
theoretical asymptotic minus 5/3 power law resulting from
Kolmogorov's inertial subrange model.
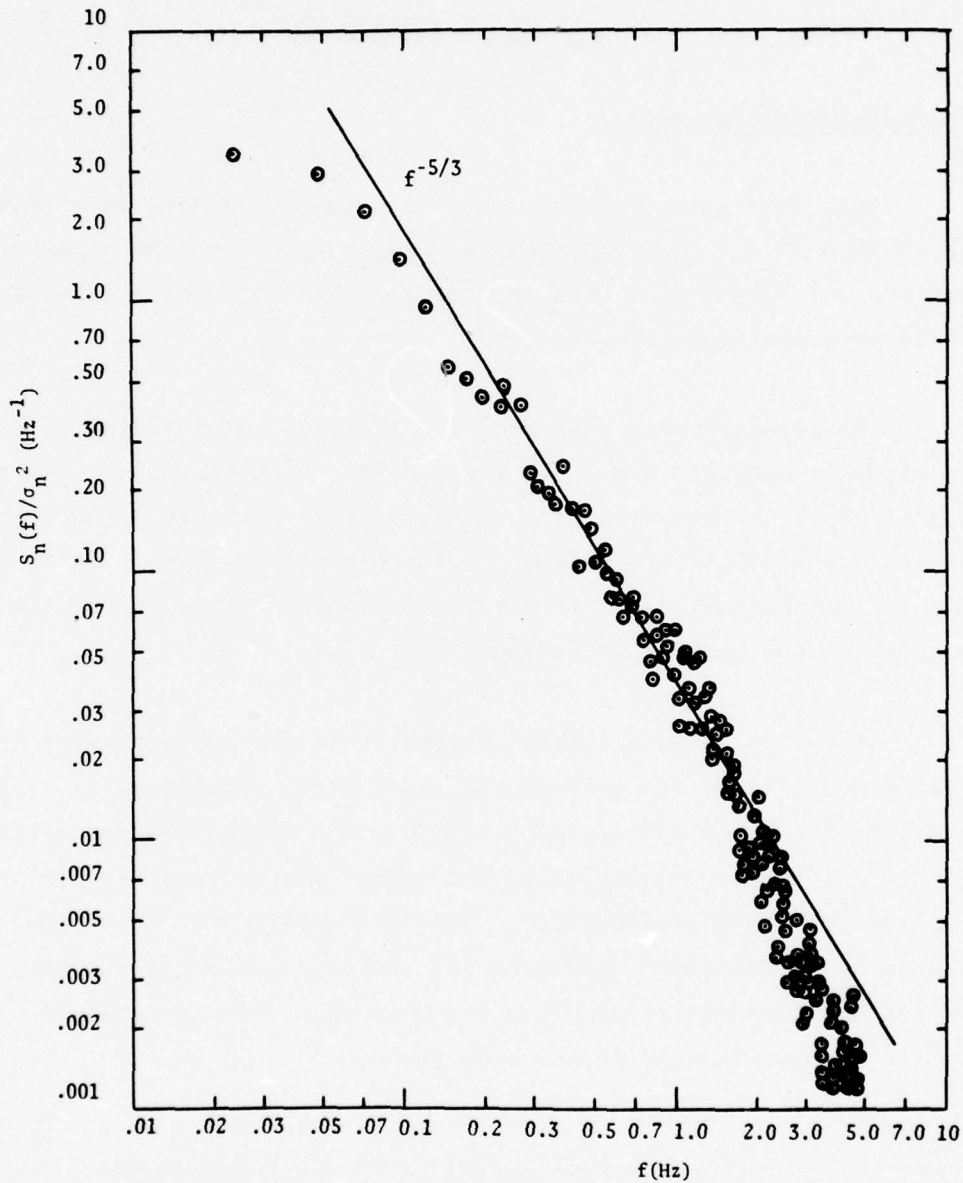
FIGURE 10- Typical refractive index power spectrum $S_n(f)/\sigma_n^2$ computed from a single 8-min long record sampled at a rate of 10 Hz. Folding or Nyquist frequency is 5 Hz and elementary frequency band 0.02 Hz. Heating power was 6.0 kW. Solid line is theoretical asymptotic minus 5/3 power law resulting from Kolmogorov's inertial subrange model.

4.0 IRRADIANCE STATISTICS

4.1 Irradiance Measurements

The light source is a 50-mW He-Ne laser radiating at a wave length $\lambda=632.8$ nm. A beam expander is used to vary the beam diameter between 1.5 and 50 mm. All data reported in this document were obtained with a 25-mm diameter collimated beam.

The irradiance is measured with a silicon photo-detector having a 1-mm diameter aperture and a 15° field of view. Measurements are made underwater where the detector can probe the laser beam along the vertical axis. The bandwidth of the photo-detector electronic circuit is 50 kHz, which is more than sufficient to cover the complete range of scintillation frequencies in the simulation medium.

Figure 11 shows a typical recording of the instantaneous irradiance measured on the axis of the laser beam, collimated to a 25-mm diameter, at a propagation distance $z=3.40$ m and for a turbulence strength $C_n=0.96\times10^{-4}$ $m^{-1/3}$. Qualitatively, this recording is very similar to what is observed in the atmosphere. The frequencies are, of course, smaller in the simulation experiment but the signal clearly exhibits the same sharp and intense irradiance peaks that are characteristic of optical wave scintillation in the atmosphere.
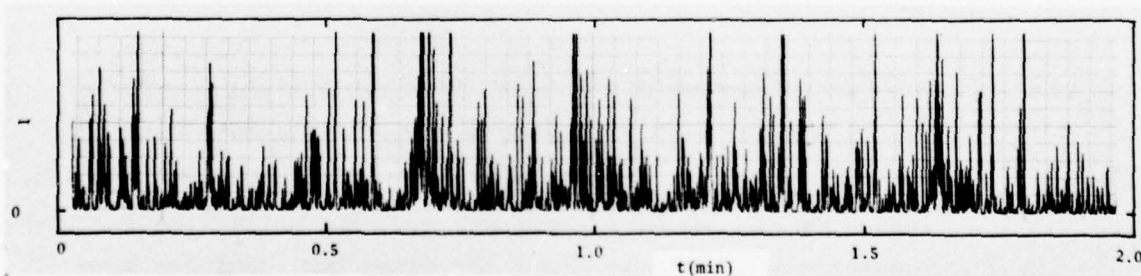

FIGURE 11- Typical time-recording of instantaneous on-axis irradiance. $2\sigma_\chi=3.5$.

4.2 Irradiance Probability Distribution

A consensus on the form of the probability distribution of the
irradiance fluctuations of optical waves propagating in the turbulent
atmosphere has not yet been reached (Ref. 19). Early theoretical models
incorporated the assumption that the irradiance fluctuations had a log-
normal distribution. This hypothesis has received wide support in
subsequent developments. However, recent numerical calculations show
that the log-normal hypothesis is inconsistent in the region of saturation
of the irradiance variance (Refs. 20-21). This was theoretically
demonstrated in Refs. 22-23 which also show that the hypothesis of
normal distribution of the wave amplitude alternatively constitutes a
plausible and consistent approximation. Data obtained from the present
simulation experiment and reported in Ref. 22 tend to corroborate the
hypothesis of a normal distribution. However, since there is no general
agreement on this subject, these data cannot be used here for the purpose
of establishing the structural similarity between turbulence in our
laboratory experiment and turbulence in the lower atmosphere.

4.3 Log-Irradiance Frequency Spectrum

Typical frequency spectra of the logarithm of the irradiance,
denoted $S_{\ell n I}(f)$, are shown in Figs. 12 and 13. The spectrum of Fig. 12
was computed from a single 43-s long record taken on the beam axis at a
distance z=1.25 m and discretely sampled at a rate of 120 Hz. In the
case of Fig. 13, the record length, propagation distance and sampling
rate are respectively 25s, 3.40 m and 200 Hz. The elementary frequency
bandwidth or frequency resolution is 0.5 Hz in both cases and
$C_n = 0.96 \times 10^{-4}$ m$^{-1/3}$.

Theoretical expressions for the temporal frequency spectra of
the log-irradiance are given by Tatarskii (Refs. 1-2) and Clifford
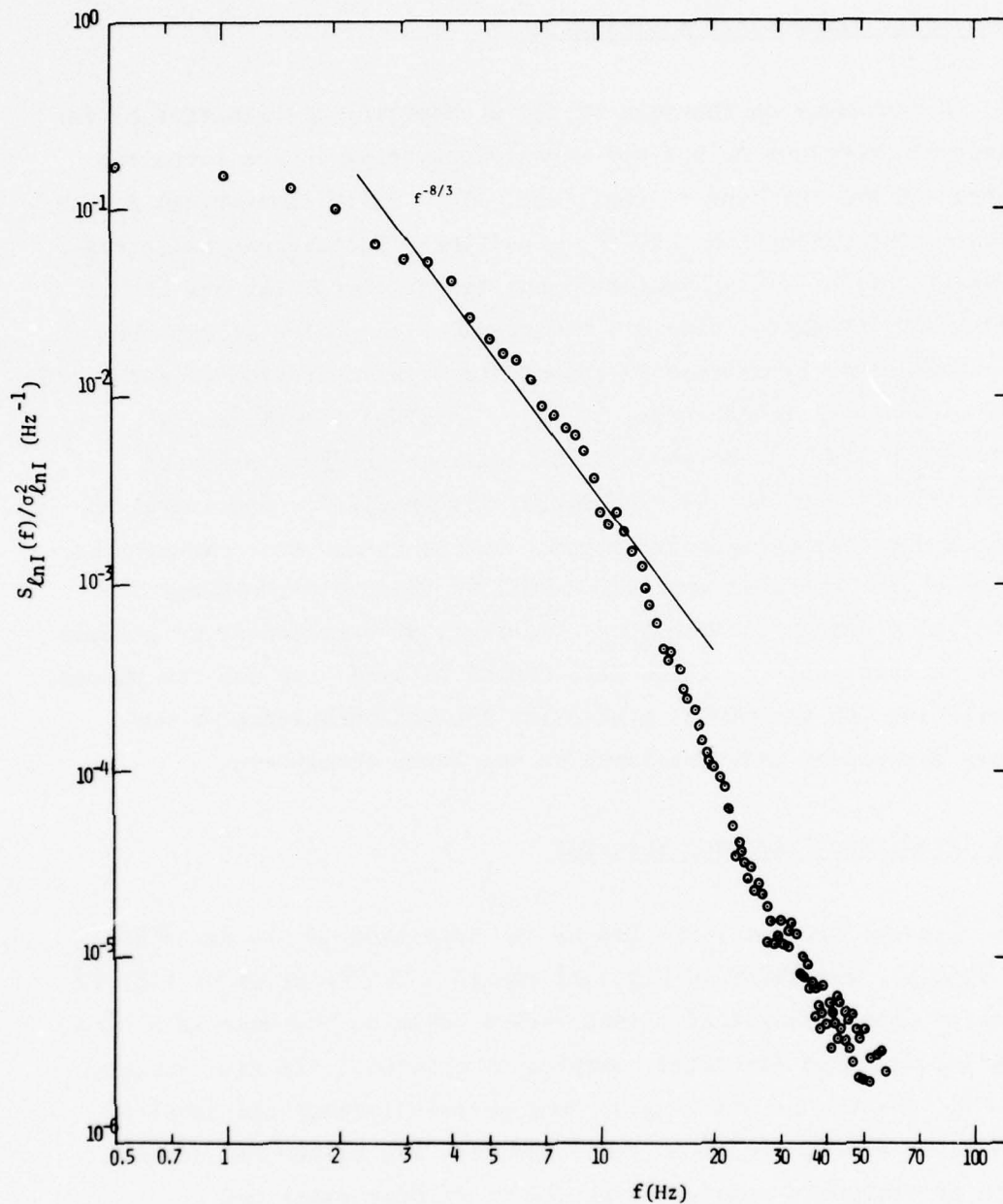(Ref. 24) for plane and spherical waves respectively. A common feature

FIGURE 12- On-axis log-irradiance power spectrum $S_{\ell nI}/\sigma^2_{\ell nI}$ computed from a single 43-sec long record sampled at a rate of 120 Hz. Folding or Nyquist frequency is 60 Hz and elementary frequency band 0.5 Hz. Solid line is theoretical asymptotic minus 8/3 power law resulting from Kolmogorov's inertial subrange model. $2\sigma_\chi = 1.4$.
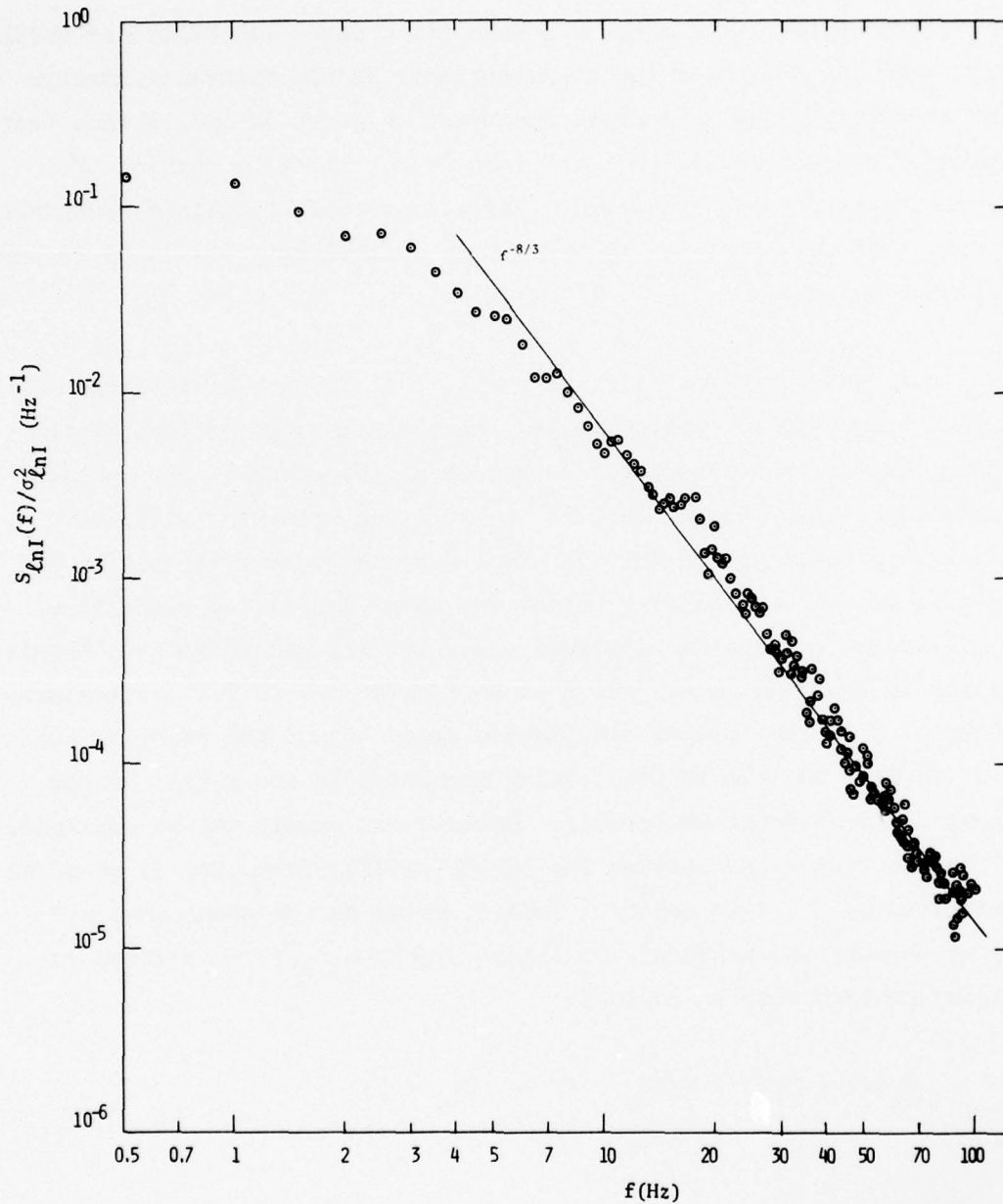
FIGURE 13- On-axis log-irradiance power spectrum $S_{\ell nI}/\sigma^2_{\ell nI}$ computed from a single 25-sec long record sampled at a rate of 200 Hz. Folding or Nyquist frequency is 100 Hz and elementary frequency band 0.5 Hz. Solid line is theoretical asymptotic minus 8/3 power law resulting from Kolmogorov's inertial subrange model. $2\sigma_X = 3.5$.

of these expressions is a minus 8/3 asymptotic power law behaviour which results from the 2/3 power law characteristic of the inertial subrange of the refractive index structure function. Figures 12 and 13 show that the minus 8/3 power law is well verified over a sizeable portion of their respective frequency domain. Therefore, these results demonstrate once more that the simulated turbulence is sufficiently developed to have an inertial subrange.

It is clear from Figs. 12 and 13 that the log-irradiance frequency spectrum, in particular the inertial subrange portion of the spectrum, shifts toward higher frequencies and broadens as propagation distance increases. Again, this is in excellent agreement with the theoretical predictions of Ref. 25 which demonstrate a shift and a broadening of the log-irradiance spectrum under increasing turbulence strength and/or propagation distance. In Fig. 12, the folding or Nyquist frequency is equal to 60 Hz, which is sufficiently high for the measured spectrum to show the steeper dissipation range beyond the inertial sub-range. In Fig. 13, the 100-Hz folding frequency is too small for the dissipation range to be noticeable. However, it should not be concluded that the inertial range reaches the 100-Hz folding frequency as seems to be indicated by the data points. Indeed, owing to the phenomenon of aliasing whereby the measured, or alias, spectrum $S_a(f)$ is related to the true spectrum $S(f)$ as follows:

$$S_a(f) = S(f) + S(2f_n - f) + S(2f_n + f)$$
$$+ S(4f_n - f) + S(4f_n + f) + \ldots, \qquad (14)$$

the results near the folding frequency f_n are the sums of contributions at frequencies f and $(2f_n - f)$ which are symmetrically located about f_n (it is assumed here that contributions at frequencies much higher than f_n are negligible). Hence, the observation that the measured spectrum near

f_n = 100 Hz follows the minus 8/3 power law indicates that the true spectrum
is actually smaller in that neighbourhood. Note that $S(f_n) \simeq S_a(f_n)/2$.
This fastest decay at higher frequencies is of course consistent with the
theory on the dissipation range. Higher sampling frequencies were
considered but, owing to the limited 5120-word capacity of the data acqui-
sition system, the resulting record was too short to represent a reliable
statistical sample of the turbulent irradiance.

In summary, the data on the log-irradiance frequency spectra give
additional evidence that the structure of the simulated turbulence has an
inertial subrange. Also, the shift of the spectrum toward higher frequencies
and the frequency broadening with propagation distance are in excellent
agreement both with theory and atmospheric data.

4.4 Irradiance Standard Deviation

The normalized irradiance standard deviation is defined as
follows:

$$\beta = [<I^2> \, / \, <I>^2 \, -1]^{\frac{1}{2}} \tag{15}$$

where I is the instantaneous irradiance measured at one point. Because β
is probably the easiest quantity to measure, it has been extensively used
to characterize scintillation phenomena and to verify theoretical models.
Despite the relatively large data spread between and within sets of data,
the following conclusions are widely accepted: 1) the theoretical first order
expression for the log-amplitude standard deviation, σ_χ, is well corroborated
at small propagation distance and/or turbulence strength; 2) the measured
normalized irradiance standard deviation reaches a maximum value near
$\sigma_\chi \approx 1.5$, decreases slightly beyond this maximum and then appears to
saturate at a constant value of the order of unity; and 3) the expression

for σ_χ constitutes a relevant propagation scale of scintillation phenomena; $\sigma_\chi \stackrel{<}{\sim} 1$ is called the weak scintillation region and $\sigma_\chi \stackrel{>}{\sim} 1$, the strong scintillation region. For infinite plane waves, σ_χ is given by the following equation (Ref. 2):

$$\sigma_\chi = 0.557 \ k^{7/12} \ C_n \ n_o^{-1} \ z^{11/12}, \tag{16}$$

where $k = n_o \omega / c$ is the radiation wave number, n_o the unperturbed index of refraction, ω the angular frequency of the source, and c the speed of light in free space.

The normalized irradiance standard deviation measured on the beam axis for three different values of turbulence strength is plotted in Fig. 14 as a function of the theoretical scaling parameter $2\sigma_\chi$. The reproducibility of these data is within ±10% which results mostly from limitations of the measuring equipment to process high peak voltages. Figure 11 shows that the irradiance signal has very intense peaks; the crest factor with respect to its RMS value is typically of the order of 10 in the strong scintillation region but it often reaches a level as high as 20. Consequently, to process these high peak voltages, the RMS voltmeter, which is limited to a crest factor of 5 at full-scale; must be operated below approximately 1/3 of full-scale where the manufacturer's specifications give an accuracy of the order of ±10% of the RMS output.

Comparison of the simulation data with the plane wave first-order solution, plotted as a solid curve in Fig. 14, reveals that the theoretical scaling formula given by σ_χ is inadequate in the weak scintillation region. The predicted scale is too short by at least a factor of 2. This apparent discrepancy is easily explained if one recalls that equation (16) is obtained under the condition $\ell_o \ll \sqrt{\lambda z} \ll L_o$, where ℓ_o and L_o are the inner and outer scales of turbulence, λ the radiation wave length and z the propagation distance. In the atmosphere, this condition is almost always

satisfied for optical and infrared waves. However, in our laboratory experiment, $\sqrt{\lambda z} \gtrsim \ell_o$ requires that z be greater than approximately 2.5 m whereas most weak scintillation data of Fig. 14 are for $z < 2.5$ m. Hence, expression (16) should be replaced by the geometrical-optics solution valid under the condition $\sqrt{\lambda z} \ll \ell_o$. The geometrical-optics expression for the log-amplitude standard deviation of an infinite plane wave is derived in Ref. 2 and is given by:

$$\sigma_g = 1.79 \ C_n \ n_o^{-1} \ \ell_o^{-7/6} \ z^{3/2} \tag{17}$$

The definition of the inner scale is somewhat qualitative and therefore ℓ_o cannot be measured with precision. The value chosen here is $\ell_o = 1.8$ mm which is given by the approximate point at which the 2/3 power law of the measured refractive index structure functions shown in Figs. 6-8 becomes applicable. Although ℓ_o should vary with the heating power as it depends on the inverse 1/4 power of the turbulent energy dissipation rate, this dependence is so weak that the approximation of a constant ℓ_o is well justified for the range of experimental conditions summarized in Table I. The weak scintillation data are plotted versus $2\sigma_g$ in Fig. 15 and compared to the first-order geometrical-optics solution given by:

$$\beta^2_g = \exp(4\sigma_g^2) - 1. \tag{18}$$

The agreement with equation (18) is very good up to $2\sigma_g = 0.6$. Therefore, the discrepancy noted in Fig. 14 is not real but only due to the use of the improper scaling formula. This result is very gratifying and is yet another proof of the consistency of our simulation approach in that the theoretically based differences between the laboratory and the atmospheric conditions are very well corroborated.

The differences between the simulation medium and the atmosphere disappear for $\sqrt{\lambda z} \gtrsim \ell_o$. For the case of Fig. 14, this corresponds to $2\sigma_\chi \gtrsim 3$. The simulation results in this region are in excellent agreement with the atmospheric data, e.g. those of Refs. 26 and 27. In particular, the maximum of the β-curve occurs at about the same distance $2\sigma_\chi \simeq 3.5$ and has approximately the same numerical value equal to 1.3 ± 0.1. Furthermore, as σ_χ increases beyond this maximum, β slowly decreases (supersaturation) with a slope similar to that observed in the atmosphere and then appears to saturate at a value close to unity for $2\sigma_\chi \gtrsim 10$, also in accordance with atmospheric observations and theoretical predictions (Refs. 13, 22, 23 and 28). Therefore, Fig. 14 shows that the simulation data obey the same scaling formula σ_χ as do the atmospheric data when the condition $\sqrt{\lambda z} \gtrsim \ell_o$ is satisfied.

In summary, our simulation experiment does reproduce on a laboratory scale and in accordance with theoretical scaling laws the effects of atmospheric turbulence on optical and infrared wave propagation: σ_g is the proper scaling formula for $\sqrt{\lambda z} \lesssim \ell_o$ whereas σ_χ applies for $\sqrt{\lambda z} \gtrsim \ell_o$.
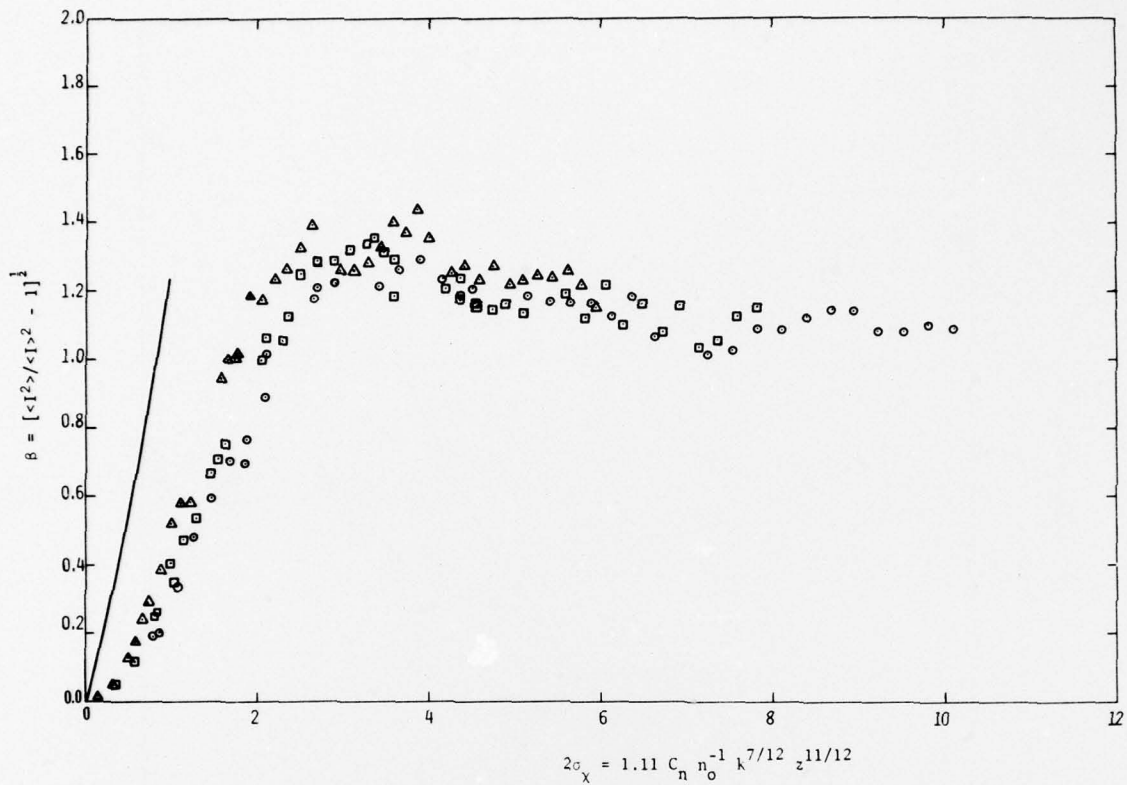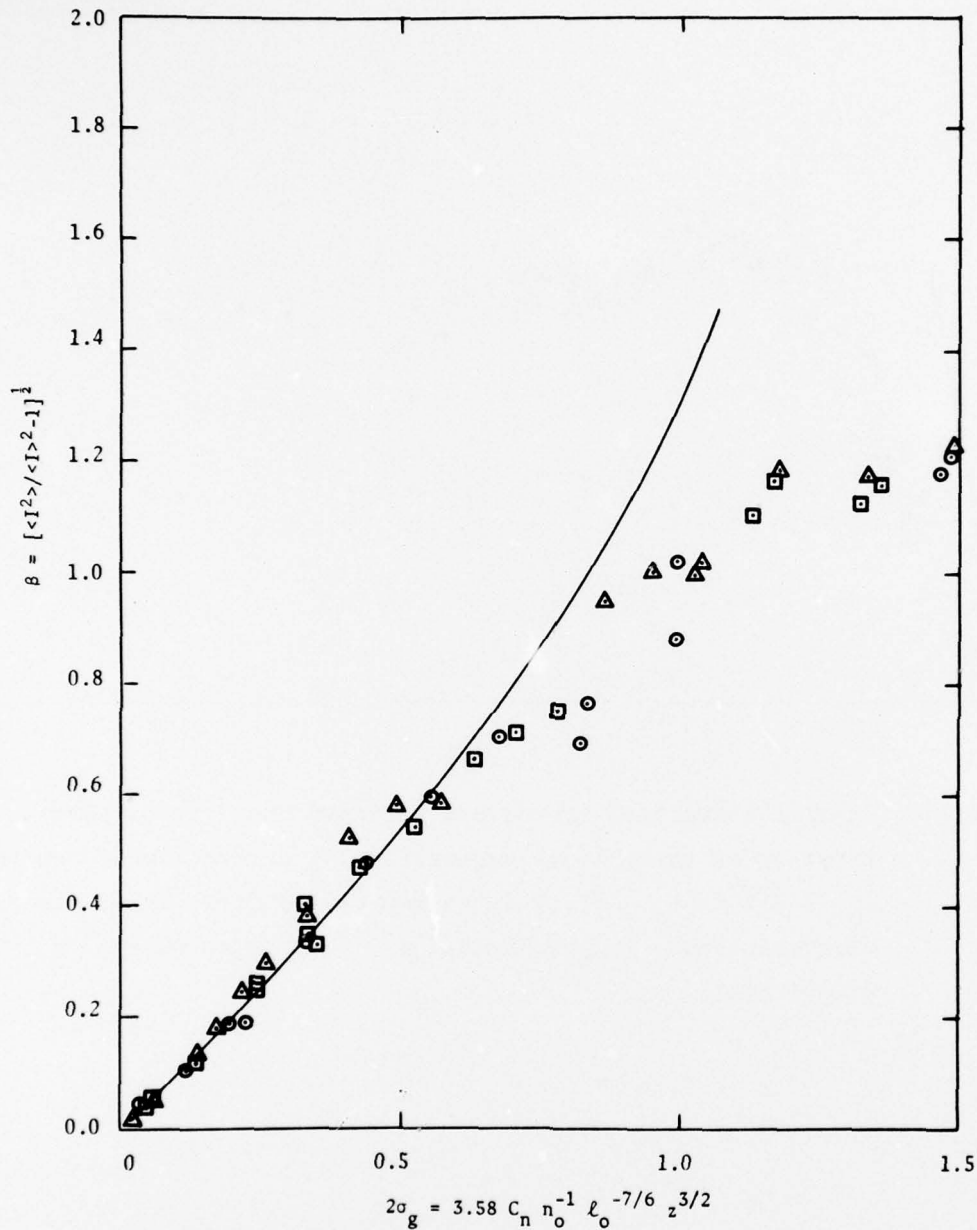
FIGURE 14- On-axis normalized irradiance standard deviation β versus first-order theoretical expression $2\sigma_\chi$ derived under condition $\ell_o \ll \sqrt{\lambda z} \ll L_o$. Solid curve represents first-order plane wave solution. $\triangle : C_n = 0.73 \times 10^{-4}$ $m^{-1/3}$; $\square : C_n = 0.96 \times 10^{-4}$ $m^{-1/3}$; $0 : C_n = 1.24 \times 10^{-4}$ $m^{-1/3}$.

FIGURE 15- On-axis normalized irradiance standard deviation β in weak
scintillation region versus first-order theoretical expression
$2\sigma_g$ derived from geometrical optics, i.e. $\sqrt{\lambda z} \ll \ell_o$. Solid
curve represents first-order plane wave solution.
$\triangle : C_n = 0.73 \times 10^{-4}$ $m^{-1/3}$; $\square : C_n = 0.96 \times 10^{-4}$ $m^{-1/3}$; $0 : C_n = 1.24 \times 10^{-4}$ $m^{-1/3}$.

5.0 <u>CONCLUSIONS</u>

A very simple procedure to simulate atmospheric turbulence for optical and infrared propagation studies was demonstrated. On the one hand, measurements in the simulation medium show that: 1) the index structure function obeys the 2/3 power law of the Kolmogorov's theoretical model, and 2) the frequency spectrum of the turbulent index has the corresponding minus 5/3 frequency dependence. These power laws, observed for all conditions studied, prove that the simulated turbulence has an inertial subrange which is necessary to have similarity of structure with turbulence in the lower atmosphere. On the other hand, measurements of the turbulent irradiance on the axis of a 25-mm diameter collimated laser beam propagating in the simulation medium demonstrate that: 1) the frequency spectrum of the logarithm of the irradiance has the minus 8/3 frequency dependence derived from the inertial subrange power law of the refractive index structure function and observed in the atmosphere, 2) the irradiance standard deviation follows the theoretical first-order predictions in the weak scintillation region and agrees very well with the predicted saturation level and the atmospherically observed super-saturation phenomenon in the strong scintillation region, and 3) the simulated scintillation phenomena obey the same scaling laws as in the atmosphere with the characteristic propagation distances typically reduced by a factor of 300 to 400.

In summary, the structure of the artificially produced turbulence is similar to that of the lower atmosphere and the evidence obtained from irradiance data is sufficient to conclude that the apparatus described in this document constitutes a very practical and accurate simulation, on a laboratory scale, of the effects of atmospheric turbulence on the propagation of optical and infrared laser beams. The advantages of being able to reproduce and control atmospheric conditions in a laboratory environment are self-evident. Our immediate plans are to use the facility to gather the specialized data necessary to verify and support the constitutive hypotheses

of our model for optical and infrared wave propagation in turbulent media outlined in Ref. 6. Also, an experiment is being planned to simulate the simultaneous action of thermal blooming and turbulence on the propagation of intense laser beams.

6.0 ACKNOWLEDGMENTS

REFERENCES

1. V.I. Tatarskii, "Wave Propagation in a Turbulent Medium" (Dover Publications, New York, 1967).

2. V.I. Tatarskii, "The Effects of the Turbulent Atmosphere on Wave Propagation", National Technical Information Service, U.S. Dept. of Commerce, Springfield, Va. (1971). UNCLASSIFIED

3. H.T. Yura, "Physical model for strong optical-amplitude fluctuations in a turbulent medium", J. Opt. Soc. Am., Vol. 64, No. 1, pp. 59-67 (1974).

4. S.F. Clifford, G.R. Ochs and R.S. Lawrence, "Saturation of optical scintillation by strong turbulence", J. Opt. Soc. Am., Vol. 64, No. 2, pp. 148-154 (1974).

5. R.L. Fante, "Some New Results on Propagation of Electromagnetic Waves in Strongly Turbulent Media", AFCRL-TR-74-0570 (1974). UNCLASSIFIED

6. L.R. Bissonnette, "A Semi-Empirical Closure Theory of Optical and IR Wave Propagation in Turbulent Media", DREV Report 708/74, Sept. 1974. UNCLASSIFIED

7. O. Rossignol, "Simulation numérique de la défocalisation thermique d'un faisceau laser intense", CRDV Rapport 4029/76, February 1976, UNCLASSIFIED

8. L.R. Bissonnette, "Steady State Thermal Blooming of Multipulse Laser Beams", DREV Report 4067/77, February 1977, UNCLASSIFIED

9. H.M. Dobbins and E.R. Peck, "Change of refractive index of water as a function of temperature", J. Opt. Soc. Am., Vol. 63, No. 3, pp. 318-320 (1973).

10. J.L. Lumley and H.A. Panofsky, "The Structure of Atmospheric Turbulence", Monographs and Texts in Physics and Astronomy, Vol. 12 (Interscience Publishers, John Wiley and Sons, New York 1964).

11. N.K. Vinnichenko, N.Z. Pinus, S.M. Shmeter and G.N. Shur, "Turbulence in the Free Atmosphere", translated from Russian (Consultants Bureau, New York 1973).

12. R.S. Lawrence, G.R. Ochs and S.F. Clifford, "Measurements of Atmospheric Turbulence Relevant to Optical Propagation", J. Opt. Soc. Am., Vol. 60, No. 6, pp. 826-830 (1970).

13. J.R. Kerr, R.A. Elliot and P.A. Pincus, "Propagation of Multiwavelength Laser Radiation Through Atmospheric Turbulence", National Technical Information Service, Springfield, Va., Order No. AD-A003-340 (1974). UNCLASSIFIED

14. G.K. Batchelor, "The Theory of Homogeneous Turbulence" (Cambridge) University Press, London 1960).

15. G.K. Born, R. Bogenberger, K.D. Erben, F. Frank, F. Mohr and G. Sepp, "Phase-front distortion of laser radiation in a turbulent atmosphere", Appl. Opt., Vol. 14, No. 12, pp. 2857-2863 (1975).

16. R.B. Blackman and J.W. Tukey, "The Measurement of Power Spectra", Section B.13 (Dover Publications, New York 1958).

17. J.I. Davis, "Consideration of Atmospheric Turbulence in Laser Systems Design", Appl. Opt., Vol. 5, No. 1, pp. 139-147 (1966).

18. C.A. Friehe, J.C. LaRue, F.H. Champagne, C.H. Gibson and G.F. Dreyer, "Effects of temperature and humidity fluctuations on the optical refractive index in the marine boundary layer", J. Opt. Soc. Am., Vol. 65, No. 12, pp. 1502-1511 (1975).

19. H.T. Yura, "Summary of Session III on Coherent Propagation, p. DIII-3, AGARD-CP-183 on Optical Propagation in the Atmosphere (1975), UNCLASSIFIED

20. T.-i. Wang and J.W. Strohbehn, "Log-normal paradox in atmospheric scintillations", J. Opt. Soc. Am., Vol. 64, No. 5, pp. 583-591 (1974).

21. T.-i. Wang and J.W. Strohbehn, "Perturbed log-normal distribution of irradiance fluctuations", J. Opt. Soc. Am., Vol. 64, No. 7, pp. 994-999 (1974).

22. L.R. Bissonnette, "Log-Normal Probability Distribution of Strong Irradiance Fluctuations: an Asymptotic Analysis", Paper No. 19, AGARD-CP-183 on Optical Propagation in the Atmosphere (1975), UNCLASSIFIED

23. L.R. Bissonnette, "Probability Distribution and Asymptotic Variance of Strong Irradiance Fluctuations of Optical Waves in Turbulent Media", DREV Report 4042/75, October 1975, UNCLASSIFIED

24. S.F. Clifford, "Temporal-Frequency Spectra for a Spherical Wave Propagating through Atmospheric Turbulence", J. Opt. Soc. Am., Vol. 61, No. 10, pp. 1285-1292 (1971).

25. H.T. Yura, "Temporal-frequency spectrum of an optical wave propagating under saturation conditions", J. Opt. Soc. Am., Vol. 64, No. 3, pp. 357-359 (1974).

26. R.L. Fante, "Irradiance scintillation: Comparison of theory with experiment", J. Opt. Soc. Am., Vol. 65, No. 5, pp. 548-550 (1975).

27. A.M. Prokhorov, F.V. Bunkin, K.S. Gochelashvily, and V.I. Shishov, "Laser Irradiance Propagation in Turbulent Media", Proc. of the IEEE, Vol. 63, No. 5, pp. 790-811 (1975).

28. J.R. Kerr, "Turbulence Effects on Target Illumination by Laser Transmitter: Unified Analysis and Experimental Verification", Paper No. 20, AGARD-CP-183 on Optical Propagation in the Atmosphere (1975), UNCLASSIFIED.

DREV R-4075/77 (UNCLASSIFIED)

Bureau- Recherche et Développement, Ministère de la Défense nationale, Canada.
CRDV, C.P. 880, Courcelette, Qué. GOA 1R0

"Laboratory Simulation of Atmospheric Turbulence for Optical Propagation Studies"
par L.R. Bissonnette

On démontre qu'une cuve remplie d'eau de 1.5 m de longueur sur 40 cm de largeur et 60 cm de profondeur, réchauffée par le bas et refroidie par le haut, constitue une technique simple pour simuler avec précision et à l'échelle du laboratoire l'effet des turbulences atmosphériques sur la propagation des ondes lumineuses. L'indice de réfraction possède une structure de turbulence similaire à celle de l'atmosphère; plus particulièrement, le modèle de Kolmogorov relatif au sous-domaine inertiel est très bien vérifié. On retrouve dans le milieu de simulation les mêmes particularités que dans l'atmosphère en ce qui a trait à la densité spectrale de l'intensité lumineuse et aux phénomènes de saturation et supersaturation de la variance de l'intensité. La loi d'échelle est la même dans les deux cas et les distances caractéristiques de propagation sont typiquement réduites par un facteur 300 à 400. (NC)

DREV R-4075/77 (UNCLASSIFIED)

Bureau- Recherche et Développement, Ministère de la Défense nationale, Canada.
CRDV, C.P. 880, Courcelette, Qué. GOA 1R0

"Laboratory Simulation of Atmospheric Turbulence for Optical Propagation Studies"
par L.R. Bissonnette

On démontre qu'une cuve remplie d'eau de 1.5 m de longueur sur 40 cm de largeur et 60 cm de profondeur, réchauffée par le bas et refroidie par le haut, constitue une technique simple pour simuler avec précision et à l'échelle du laboratoire l'effet des turbulences atmosphériques sur la propagation des ondes lumineuses. L'indice de réfraction possède une structure de turbulence similaire à celle de l'atmosphère; plus particulièrement, le modèle de Kolmogorov relatif au sous-domaine inertiel est très bien vérifié. On retrouve dans le milieu de simulation les mêmes particularités que dans l'atmosphère en ce qui a trait à la densité spectrale de l'intensité lumineuse et aux phénomènes de saturation et supersaturation de la variance de l'intensité. La loi d'échelle est la même dans les deux cas et les distances caractéristiques de propagation sont typiquement réduites par un facteur 300 à 400. (NC)

DREV R-4075/77 (UNCLASSIFIED)

Bureau- Recherche et Développement, Ministère de la Défense nationale, Canada.
CRDV, C.P. 880, Courcelette, Qué. GOA 1R0

"Laboratory Simulation of Atmospheric Turbulence for Optical Propagation Studies"
par L.R. Bissonnette

On démontre qu'une cuve remplie d'eau de 1.5 m de longueur sur 40 cm de largeur et 60 cm de profondeur, réchauffée par le bas et refroidie par le haut, constitue une technique simple pour simuler avec précision et à l'échelle du laboratoire l'effet des turbulences atmosphériques sur la propagation des ondes lumineuses. L'indice de réfraction possède une structure de turbulence similaire à celle de l'atmosphère; plus particulièrement, le modèle de Kolmogorov relatif au sous-domaine inertiel est très bien vérifié. On retrouve dans le milieu de simulation les mêmes particularités que dans l'atmosphère en ce qui a trait à la densité spectrale de l'intensité lumineuse et aux phénomènes de saturation et supersaturation de la variance de l'intensité. La loi d'échelle est la même dans les deux cas et les distances caractéristiques de propagation sont typiquement réduites par un facteur 300 à 400. (NC)

DREV R-4075/77 (UNCLASSIFIED)

Bureau- Recherche et Développement, Ministère de la Défense nationale, Canada.
CRDV, C.P. 880, Courcelette, Qué. GOA 1R0

"Laboratory Simulation of Atmospheric Turbulence for Optical Propagation Studies"
par L.R. Bissonnette

On démontre qu'une cuve remplie d'eau de 1.5 m de longueur sur 40 cm de largeur et 60 cm de profondeur, réchauffée par le bas et refroidie par le haut, constitue une technique simple pour simuler avec précision et à l'échelle du laboratoire l'effet des turbulences atmosphériques sur la propagation des ondes lumineuses. L'indice de réfraction possède une structure de turbulence similaire à celle de l'atmosphère; plus particulièrement, le modèle de Kolmogorov relatif au sous-domaine inertiel est très bien vérifié. On retrouve dans le milieu de simulation les mêmes particularités que dans l'atmosphère en ce qui a trait à la densité spectrale de l'intensité lumineuse et aux phénomènes de saturation et supersaturation de la variance de l'intensité. La loi d'échelle est la même dans les deux cas et les distances caractéristiques de propagation sont typiquement réduites par un facteur 300 à 400. (NC)

DREV R-4075/77 (UNCLASSIFIED)

Research and Development Branch, Department of National Defence, Canada.
DREV, P.O. Box 880, Courcelette, Qué. G0A 1R0

"Laboratory Simulation of Atmospheric Turbulence for Optical Propagation Studies"
by L.R. Bissonnette

Accurate simulation, on a laboratory scale, of atmospherically induced scintillation phenomena is achieved by creating an unstable vertical temperature gradient in a 1.5-m long, 40-cm wide and 60-cm deep tank filled with water. The turbulent index of refraction has a statistical structure similar to that of the atmosphere; in particular, the Kolmogorov's inertial subrange model is verified. The turbulent irradiance data in the simulation medium have the same features respecting power spectrum, saturation and supersaturation and obey the same theoretical scaling law as in the atmosphere. Typically, the characteristic propagation distances are reduced by a factor of 300 to 400. (U)